3D Numerical Simulation of Catalyst Injection into a Dense Fluidized Bed

3D Numerical Simulation of Catalyst Injection into a Dense Fluidized Bed

Z. Zeren[1,2], A. Ozel[1,2], A. Sarthou[1,2], P. Fede[1,2], H. Neau[1,2], O. Simonin[1,2]
Jean-Louis Chamayou[3], I. Ghouila[3]

[1] *Université de Toulouse :INPT, UPS ; IMFT : Allée Camille Soula, F-31400 Toulouse, France*
[2] *CNRS : Institut de Mécanique des Fluides de Toulouse, F-31400, Toulouse, France*
[3] *INEOS Chemicals Lavéra SAS: CTL/PRO Ecopolis Lavéra, BP6-13117, Lavéra, France*

Keywords: Fluidized bed, gas-solid flows, Euler/Euler approach, gas mixture properties

Abstract

In this study, the injection of catalyst particles into a dense gas-solid fluidized bed reactor is investigated using the Euler/Euler approach. Numerical simulations of horizontal catalyst+gas mixture injection through a circular-sectioned nozzle have been performed in order to study the effect of the operating conditions of an injector on the flow hydrodynamics. The study is in the context of a larger project to optimize the nozzle geometry. The nozzle is composed of two annular sections, one outer and one inner. Catalyst is injected from the central section of the nozzle with a transport gas called here "gas 1". Another gas is injected in the outer section: "gas 2".
The results show that the good dispersion of the catalyst depends highly on the ratio of the velocities in the outer and the inner sections of the nozzle.

Nomenclature

Roman letters

C_D	Drag coefficient (-)
g	Gravitational acceleration (m.s^{-2})
$I_{m\to k}$	Momentum transfer between phases m and k (kg.m^{-2}.s^{-2})
$\dot{m}^2_\alpha$	Mass flux of component α (kg.s^{-1})
M_α	Molecular weight of gas component α (kg.kmol^{-1})
q_p^2	Mean particle agitation (m^2.s^{-2})
P_g	Mean gas phase pressure (N.m^{-2})
Re_p	Particle Reynolds number (-)
$R_{k,ij}$	Mean agitation of phase k (m^2.s^{-2})
$U_{k,i}$	Mean velocity of phase k in direction i (m.s^{-1})
V_r	Mean relative velocity (m.s^{-1})

Greek letters

α_k	Volume fraction of phase k (-)
$\Theta_{k,ij}$	Molecular stress tensor (m^2.s^{-2})
μ_g	Dynamic viscosity of gas mixture (Pa.s)
ρ_k	Density of phase k (kg.m^{-3})
τ_{gp}^F	Mean gas-particle relaxation time (s)

Subscripts

g	Gas phase properties
i	ith direction component of a vector
p	Particle phase properties

Introduction

Polyethylene is a largely used thermoplastic material in many different industrial applications such as plastic packaging. It is produced basically by using the ethylene as a monomer through the polymerization reactions with very small diameter catalyst particles. The reactions are housed in a pressurized fluidized bed reactor under controlled temperature and pressure conditions. The catalyst is continuously fed into the fluidized bed and it reacts with the incoming gas from the fluidization grid to produce polyethylene. Dispersion of the catalyst in the bed is an important parameter to characterize the homogeneity of the reactions. If the catalyst accumulates in localized regions in the bed, it can lead to agglomerates formation.

In this study, the focus is on the hydrodynamics of the gas-particle flow around the injection nozzle, particularly, the effect of the operating conditions of the nozzle on the catalyst dispersion. The three-phase flow, the catalyst particles, solid particles of the bed and the gas phases, is modeled using Euler/Euler approach. The approach is based on the mean transport equations of mass and momentum for each phase and the equations are coupled through interphase transfer terms. The particle agitation is modeled using two separate transport equations for the particle kinetic energy and the fluid-particle interactions. Both particle and catalyst phases are of uniform diameter and only the fluidized particles of the bed have a back effect on the fluid phase. The turbulence of the gas phase is modeled using the $k-\varepsilon$ model. A scalar transport equation is solved to follow the behavior of these components by neglecting their diffusion. Due to the differences in their densities, local mixture density and dynamic viscosity are estimated at each point of the domain.

Mathematical Modeling

Particle phase mean transport equations of mass, momentum and energy are derived from the Boltzmann-type equation using the method of moments (Simonin, 1996). The mass balance is written as:

$$\frac{\partial}{\partial t}\alpha_k\rho_k + \frac{\partial}{\partial x_i}\alpha_k\rho_k U_{k,i} = 0 \tag{1}$$

where α_k is the volume fraction of the phase k (k=1 gas, k=2 particles, k=3 catalyst). It satisfies:

$$\sum_{k=1}^{3}\alpha_k = 1 \tag{2}$$

$U_{k,i}$ is the ith component of velocity of phase k.

Momentum balance equation writes:

$$\alpha_k\rho_k\left[\frac{\partial U_{k,i}}{\partial t} + U_{k,j}\frac{\partial U_{k,i}}{\partial x_j}\right] = -\alpha_k\frac{\partial P_g}{\partial x_i} + \alpha_k\rho_k g_i + \frac{\partial}{\partial x_j}\left[-\alpha_k\rho_k R_{k,ij} + \Theta_{k,ij}\right] + \sum_{m\neq k} I_{m\to k,i} \tag{3}$$

where P_g is the gas phase pressure.

Interphase momentum exchange term between the particles and the gas is modeled as:

$$I_{p\to g,i} = -I_{g\to p,i} = \alpha_p\rho_p\frac{V_{r,i}}{\tau_{gp}^F} \tag{4}$$

where $V_{r,i} = U_{p,i} - U_{g,i} - V_{d,i}$ represents the ith component of the mean relative between the particles and the surrounding gas. $V_{d,i}$ accounts for the drift velocity of the particles due to the turbulent transport of particles by the large scales of the flow (Balzer et al, 1996). Following Simonin (1996), it is approached by:

$$V_{d,i} = -D_{gp,ij}\left[\frac{1}{\alpha_p}\frac{\partial\alpha_p}{\partial x_j} - \frac{1}{\alpha_g}\frac{\partial\alpha_g}{\partial x_j}\right] \tag{5}$$

Fluid-particle dispersion coefficient tensor is given by:

$$D_{gp,ij} = \frac{1}{3}q_{gp}\tau_{gp}^F\delta_{ij} \tag{6}$$

where q_{gp} is the fluid-particle covariance and it is determined by solving a separate transport equation (Simonin, 1996). δ_{ij} is the Kronecker delta function which is 0 if $i \neq j$.

The characteristic timescale in (6) is determined by using a drag law approximated by:

$$\frac{1}{\tau_{gp}^F} = \frac{3}{4}\frac{\rho_g}{\rho_p}\frac{C_D\left\langle \mathrm{Re}_p\right\rangle_p}{d_p}\left\langle\left|\mathbf{u}_r\right|\right\rangle_p \tag{7}$$

with the mean drag coefficient (Gobin et al, 2003) written by:

$$C_D = \begin{cases} C_{D,WY}; & \alpha_p < 0.3 \\ \min(C_{D,WY}, C_{D,Erg}); & \alpha_p > 0.3 \end{cases} \tag{8}$$

where Ergun drag coefficient $C_{D,Erg}$ is given by:

$$C_{D,Erg} = 200\frac{\alpha_p}{\mathrm{Re}_p} + \frac{7}{3} \tag{9}$$

and the Wen&Yu drag coefficient is given by:

$$C_{D,WY} = \begin{cases} \frac{24}{\mathrm{Re}_p}\left(1 + 0.15\,\mathrm{Re}_p^{0.687}\right)\alpha_g^{-1.7}; & \mathrm{Re}_p < 1000 \\ 0.44\,\alpha_g^{-1.7}; & \mathrm{Re}_p > 1000 \end{cases} \tag{10}$$

Particle Reynolds number is defined as:

$$\mathrm{Re}_p = \alpha_g\frac{\rho_g\left\langle\left|\mathbf{u}_r\right|\right\rangle_p d_p}{\nu_g} \tag{11}$$

In the momentum equation (3), $R_{k,ij}$ is the turbulent stress tensor for $k = g$ and the particle kinetic stress tensor for $k = p$. Particle kinetic stresses represent the transport of the momentum by the particle velocity fluctuations and the collisional stress is related to the transfer of momentum by the inter-particle collisions. The modeling of the kinetic and collisional parts of the particle stress tensor is developed in the frame of the kinetic theory of the granular medium. The interstitial turbulence effects and the drag force supplement this model. Gas phase turbulent stress tensor is modeled by a Boussinesq-like approximation in the frame of the turbulent eddy-viscosity assumption. The turbulent viscosity is obtained from the separate transport equations of the turbulent kinetic energy and its dissipation. These two equations, conventionally called "$k-\varepsilon$ models", include additional terms for the two-way coupling between the particles and the gas. For the sake of brevity, these equations will not be written here. Interested reader may refer to (Simonin, 1996).

The term $\Theta_{k,ij}$ in the momentum equation represents the laminar viscous stress tensor ($k = g$) and collisional stress tensor ($k = p$). The collisional stress tensor models the exchange or destruction of the momentum between the particles during the collisions (Boelle et al., 1995).

Scalar Transport

Two scalar transport equations are solved in order to follow the components of the gas mixture. The diffusion of the species is neglected. The equation is written as:

$$\alpha_g\rho_g\frac{\partial Y_\alpha}{\partial t} + \alpha_g\rho_g U_{g,j}\frac{\partial Y_\alpha}{\partial x_j} = 0 \tag{12}$$

where Y_α is the concentration of the species, gas2 $\alpha = 1$ and gas 1 $\alpha = 2$. The concentration verifies the relation:

$$\sum_{\alpha=1}^{2} Y_\alpha = 1 \tag{13}$$

Mixture density

Assuming the gas mixture as a mixture of perfect gases, the gas phase density can be computed as a function of the local species concentration (Konan et al., 2010) using the formula:

$$\rho_g = \frac{P_g}{R_g T_g} M_g \tag{14}$$

where M_g is the molar mass of the mixture, P_g is the reference pressure inside the reactor, R_g is the universal gas constant and T_g is the local temperature. The molar mass is computed as:

$$\frac{1}{M_g} = \sum \frac{Y_\alpha}{M_\alpha} \tag{15}$$

where Y_α is the concentration, M_α is the molar mass of gas phase components.

Practically, the scalar transport equation (12) is solved for one of the gas phase components concentration and the second one is computed from the relation:

$$Y_2 = 1 - Y_1 \tag{16}$$

Mixture dynamic viscosity

Dynamic viscosity of the perfect gas mixture is calculated by using the formula:

$$\mu_g = \frac{\sum Y_\alpha \mu_\alpha (M_\alpha)^{1/2}}{\sum Y_\alpha (M_\alpha)^{1/2}} \tag{17}$$

Simulations Overview

3D numerical simulations are carried out using an n-fluid Euler/Euler code, which is developed and implemented in IMFT (Institut de Mécanique des Fluides de Toulouse) in a specific version known as NEPTUNE_CFD V1.08@Tlse. NEPTUNE_CFD is multiphase flow software developed in the framework of NEPTUNE project financed by CEA (Commisariat à l'Enérgie Atomique), EDF (Eléctricité de France), IRSN (Institut de Radioprotection et de Sûreté Nucléaire) and AREVA-NP.

In order to study the multiphase flow field around the injection nozzle, a fluidized bed representative geometry has been generated. As mentioned briefly in the introductory section, injection nozzle has two annular sections, one inner and one outer section. Catalyst particles are injected horizontally from the inner section via a "gas 1" carrier phase. From the outer section, "gas 2" is injected. Simulations were done with a very fine mesh around the injector in order to capture the underlying physics of the flow in this area

Two simulations have been performed. The simulations are distinguished by the mass flux rate of "gas2" $\dot{m}_{gas2}$ and of "gas1" $\dot{m}_{gas1}$ from the injection nozzle:

$$r = \frac{\dot{m}_{gas2}}{\dot{m}_{gas1}} \tag{18}$$

The first simulation is the standard case with a low ratio r and the second simulation is with a substantially high ratio. The main objective of this study is to assess the impact of the mass fluxes ratios on the catalyst dispersion.

Mesh and Geometry

In Figure 1, the geometry of the bed is shown. The dimensions are 1mx2m of a rectangular section and 4m of height. The injector can be distinguished at the lower left section of the geometry. In Figure 2, the injector is presented. As can be seen from the figure, the inner section for the catalyst injection penetrates further in the flow than the outer section for the injection of "gas2". In Figure 3, the local mesh around the injector with a perspective view is shown. The inner and outer sections of the injector where the catalyst with "gas1" and "gas2" are injected, respectively, can be seen clearly.

The mesh contains in total around 700 000 hexahedral elements. The cells are fine enough around the injectors and far from the injectors they are coarsened to reduce the cost of the simulations.

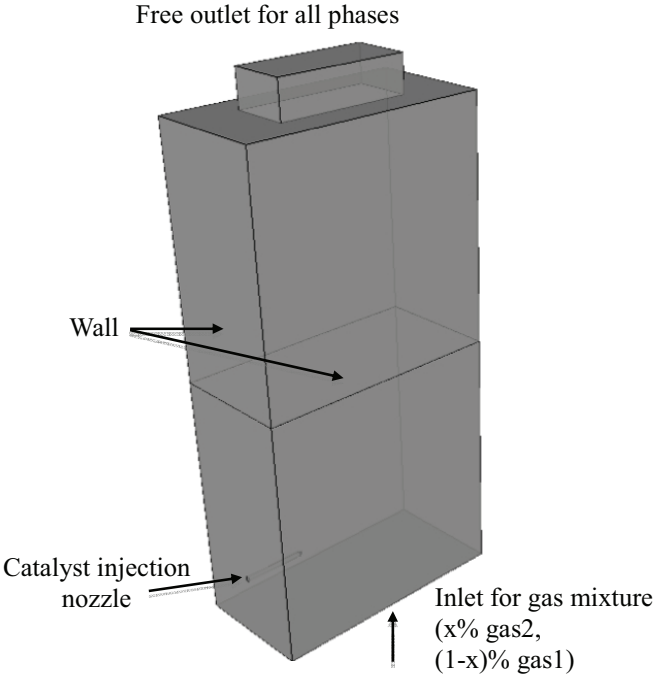

Figure 1: Configuration of the fluidized bed reactor.

Performing the Simulations and Computer Performances

Simulations are performed in two steps; the first is the

transient period including the time required for the statistical quantities of interest to become stationary (around 5s physics depending on the superficial velocity at the fluidization grid and the height of the bed) and the second is the period where the time-averaged mean of the variables has been performed (around 3s). These are primarily the concentration fields of the components of gas phase and the volume fraction fields of the catalyst and solid particles. The velocity fields are also of interest.

Simulations have been performed on a parallel platform on the supercomputer CALMIP (Toulouse). Accordingly with the number of cells, 64 cores are used (Neau et al., 2010). A typical timestep for the simulations is around $5x10^{-6}$s.

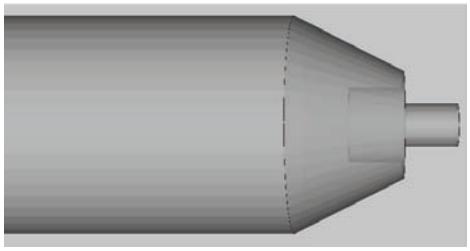

Figure 2: View close of the injection nozzle.

Initial and Boundary Conditions

At the initial state (t=0), the gas is at rest and the initial height of the particles is 2m. Initial volume fraction of particles is 0.4.

The fluidization grid (z=0) is an inlet for the gas phase with a superficial velocity of 0.65 m/s corresponding to the fluidization velocity υ_f. The gas at the grid is a mixture of x % gas2 and of (1-x)% gas1. For the particles, this section is a wall.

At the top of the bed, a free outlet surface is defined for all phases. All the vertical faces and the injector are defined as wall-type boundary conditions. Friction wall boundary condition is used for the gas phase. For the particles, following the recent study of Fede et al (2009), no-slip boundary condition is used. This condition is written in equation as:

$$\left[U_{p,i}\right]_{wall} = 0 \qquad \left[\frac{\partial q_p^2}{\partial n}\right]_{wall} = 0 \tag{19}$$

where $U_{p,i}$ is the particle mean velocity in i^{th} direction.

The outer and inner sections of the nozzle are also inlet for the components of the gas phase and the catalyst particles. As already explained above, the inner section is for the injection of the catalyst via “gas1” carrier phase and the outer section is for the injection of ”gas2”.

Material properties and operating conditions

The operating temperature of the bed ranges between 70 and 120°C and the pressure is 25bar. Solid mass of the bed is 990kg and particles are of uniform diameter ranging between 400 to 1200 µm Their density ranges between 700 to 900kg/m^3. The catalyst injected is composed of uniform diameter particles ranging between 30 and 100µm and their density ranges from 700 to 900kg/m^3.

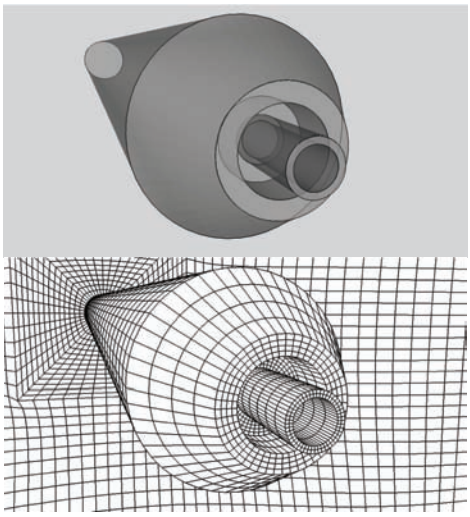

Figure 3: Perspective view of the injection nozzle and the mesh, inner and outer sections for the injection of catalyst with “gas1” and ”gas2”, respectively, can be seen.

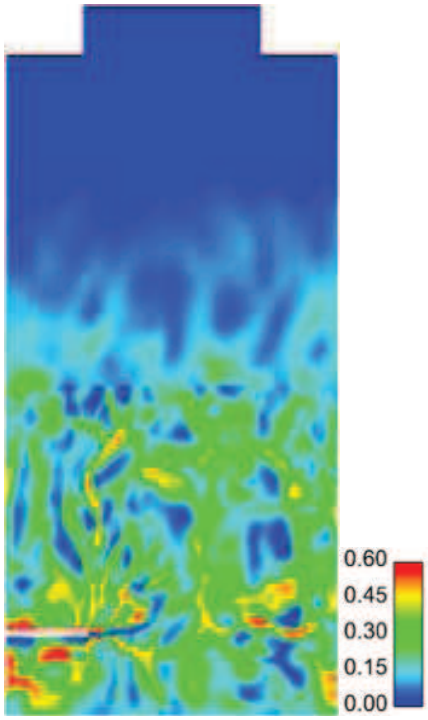

Figure 4: Field of volume fraction of solid particles of the bed, catalyst injector can be distinguished at lower part.

Results and Discussion

Effect of the mass flux ratio on the dynamics of the catalyst particles

In this section, we study the effect of increasing the mass flux ratio r on the catalyst particle concentration in the immediate vicinity of the nozzle. Simulations have been performed with no-slip boundary conditions for the particles and with friction boundary conditions for the gas phase.

Before determining the regions where the catalyst particles can meet reactive gas, we will study the dynamics of these particles due to the gas mixture velocity ratio between the inner and outer sections of the injector.

In Figure 4, the general view of a section of the bed is shown with the instantaneous volume fraction field of the solid particles to give an idea about the flow configuration, e.g., injection of catalyst into a dense bed. The particulate flow structures are clearly seen in the figure.

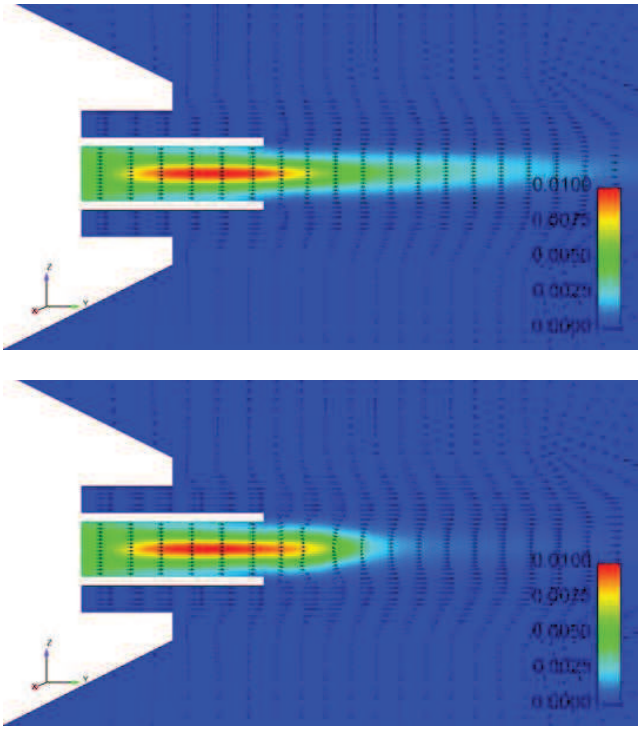

Figure 5: Concentration field of the catalyst particles and vector field of the mean axial gas mixture velocity for low mass flux (above) and for high mass flux (down).

The Figure 5 shows the spatial distribution of the concentration of catalyst particles superposed with the velocity vectors of the gas mixture. As expected, the maximum catalyst concentration is obtained at the core region inside of the injector for both cases. Towards the end of the injector, catalyst particles separate from the inner walls of the injector. It can also be remarked that in the standard case, the catalyst has some important penetration length relative to the length of the inner part of the injector.

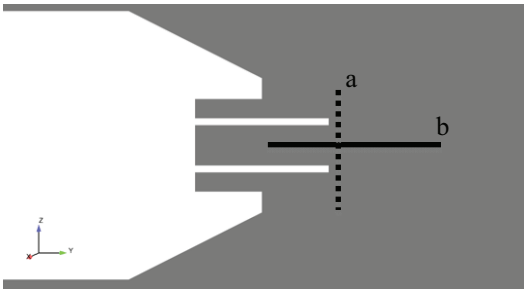

Figure 6: Positions of the lines on which the axial mean gas mixture velocity is traced on figures 7 and 8.

The gas mixture velocity field shows an intuitive behavior. For both cases, higher mass flux of “gas2” coming from the outer section of the injector compensates the low mass flux ”gas1”+catalyst mixture at the end of the region where the catalyst concentration diminishes to zero. Gas mixture velocity shows a sudden expansion at the tip of the injector, which encloses the catalyst particles into a triangular region in 2D.

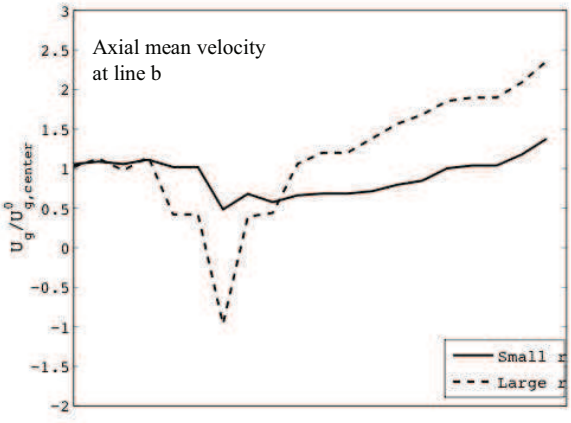

Figure 7: Axial mean gas velocity on the line b in figure 6, $U^0_{g,center}$ is the mean gas velocity at the center of the injection surface of the inner section of the nozzle.

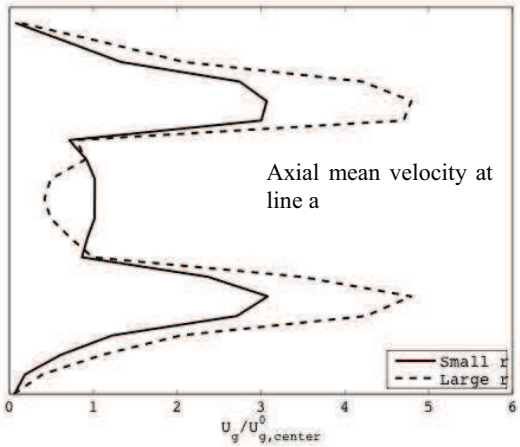

Figure 8: Axial mean gas velocity on the line a in figure 5, $U^0_{g,center}$ is the mean gas velocity at the center of the injection surface of the inner section of the nozzle.

When ”gas2” mass flux rate is increased substantially, high r, basically the flow picture is the same. The maximum of the concentration of the catalyst particles is at the similar region to the low r case and the dimension of the core region (where catalyst concentration is 0.01) is also similar in two cases. However, it can be remarked clearly that the penetration length of the catalyst diminishes.

The diminution in the penetration length of the catalyst is primarily due to the higher mass flux of “gas2” in the second case. It can be observed from the figure that due to this high flux from the outer section, the expansion of the velocity vectors is restrained and this behavior encloses the particles into a smaller region than the lower r case. Gas phase penetration is, nevertheless, larger than the standard case.

In order to quantify the effects of this increase in the mass flux, we traced the axial mean velocity (direction +y) of the

gas at the center of the inner section and at a vertical line in front of the injector; which are presented in the Figure 6. The Figure 7 and 8 present the evolution of the mean axial velocity. As seen in the Figure 7, the velocity of the gas drops suddenly to minus values at the tip of the injector. This indicates a region where the catalyst particles have a strong potential of moving into the injector due to the fact that their motion is controlled primarily by the carrier gas mixture since the catalysts have very low inertia.

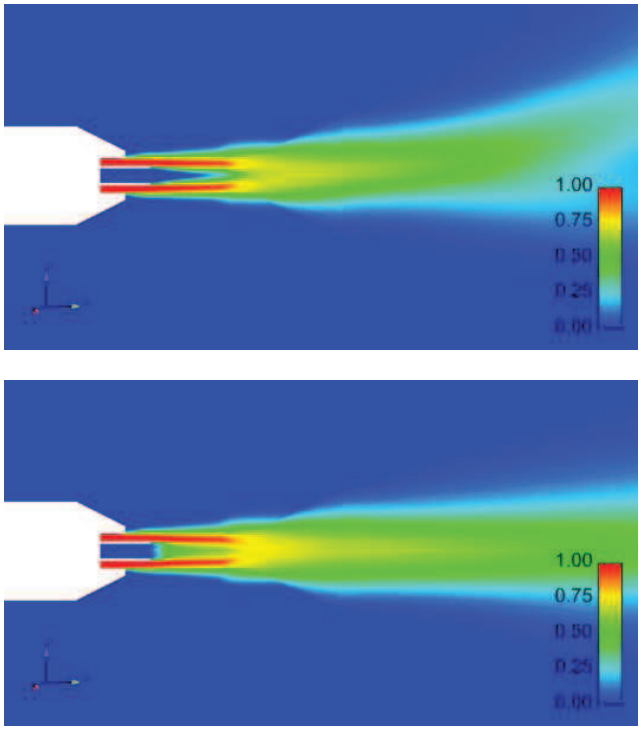

Figure 9: Mean concentration of "gas2" coming from the injector for low mass flux (above) and for high mass flux (down).

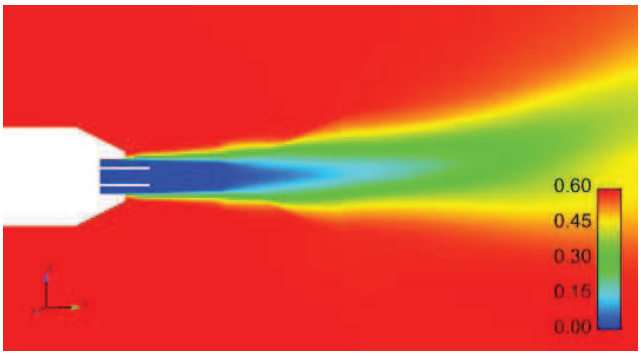

Figure 10: Mean concentration of gas2 coming from the fluidization grid for the low r case.

In figure 8, we present the axial mean gas velocity on a vertical line covering the width of the injector (line a in figure 6). It is evident from the figure that the penetration of "gas2" from the outer section is larger for the high mass flux case than the standard case.

"gas2" concentration

In this section, we study the spatial distribution of "gas2" component of the gas mixture and its covariance with the catalyst particles concentration near the injector. We study also the source of the "gas2" in front of the injector (is it from the injector or from the fluidization grid?). For the simplicity, they will be called, gas2-inj and gas2-grid, respectively.

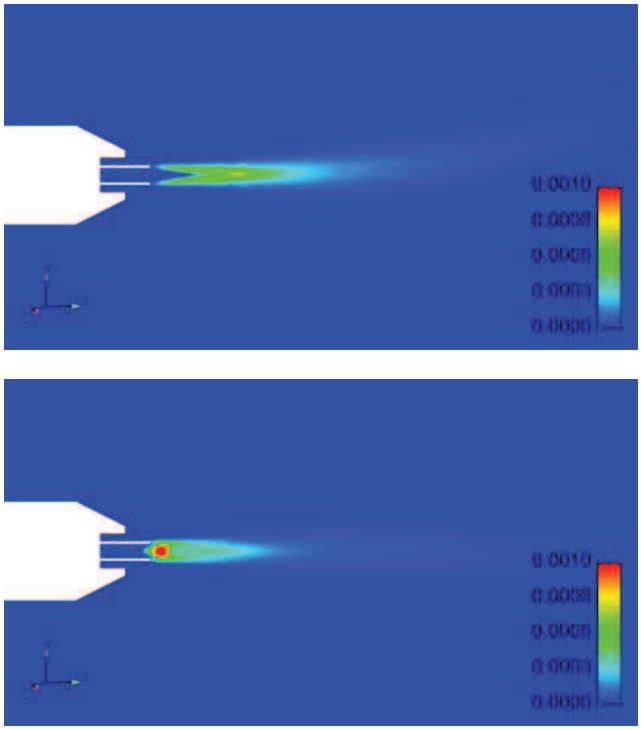

Figure 11: Mean correlation between the catalyst and "gas2" concentration (gas2-inj coming from the injector) for low mass flux (above) and for high mass flux (down).

The Figure 9 shows the mean concentration distributions of the gas2-inj for the two values of r. It is remarkable that the maximum of the gas2-inj concentrations occupies the similar regions before the injector for both cases. However, much higher concentration values (up to 0.5) are obtained at the tip of the injector due to the sudden expansion of the "gas2" coming from the outer section for the case with high r value. The Figure 10 shows the distribution of the gas2-grid only for the low r value case since the distributions are practically the same for both cases. From the figure, we can conclude that the "gas2" concentration in front of the injector coming from the grid at the bottom of the bed is negligible.

Figure 11 shows the mean covariance between the gas2-inj and the catalyst particles for both cases. In coherence with the concentration of gas2-inj shown in the Figure 9, this figure shows that the increase in the mass flux rate of the gas2 in the outer section of the injector increases the possibility of the reactions at the tip of the injector if gas2 is a reactive gas.

Figure 12 shows the covariance between the catalyst particles and the gas2-grid coming from the fluidization grid. It is evident from the figure that the possibility of reactions with the gas2-grid is rather negligible in front of the injector. Even far from the injector, it must be noted that the covariance is at least 10 times smaller than in the standard case.

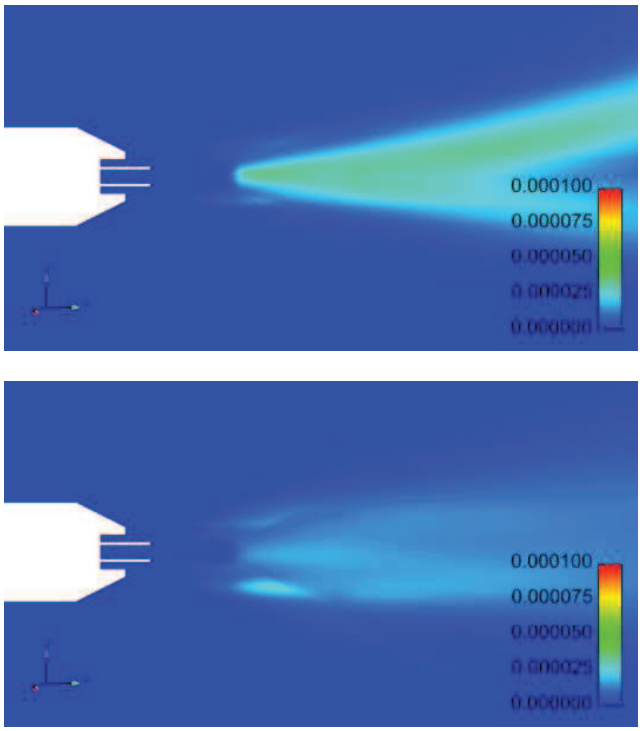

Figure 12: Mean correlation between the catalyst and gas2 concentration (gas2-grid coming from the fluidization grid) for low mass flux (above) and for high mass flux (down).

Conclusion

Three-dimensional unsteady simulations of an isothermal polymerization reactor fluidized-bed have been performed. Primarily, the concentration fields of the gas mixture components and the catalyst particles are investigated in order to study the effect of the substantially high mass flux of the gas from the outer section of the injector on the hydrodynamics of the gas-solid flow in front of the injector. The results show that the large velocity ratio (r) between the outer and inner sections of the injector leads to a stagnation point for the catalyst at the tip of the injector. It has also been shown that gas2 present near to the injector comes from the injection nozzle, not from the fluidization grid. Simulations indicate that gas2 injected from the fluidization grid does not enter the near-injection region at the tip of the nozzle.

Acknowledgements

This work was granted access to the HPC resources of CALMIP under the allocation 2012-P0111.

References

Balzer, G., Simonin, O., Flour, I., and Laviéville, J. A unifying modeling approach for the ´numerical prediction of dilute and dense gas-solid two-phase flows. In J. L. M. Kwauk (Ed.), Circulating Fluidized Bed Technology V, Beijing, pp. 432–439. Science Press (1996)

Boelle, A., Balzer, G., and Simonin, O. Second order prediction of the part-phase stress tensor of inelastic spheres in simple shear dense suspensions. In ASME Gas-Solid Flows Symposium (1995)

Fede, P., Moula, G., Ingram, I., Dumas, T. and Simonin, O. 3D numerical simulation and PEPT experimental investigation of pressurized gas-solid fluidized bed hydrodynamic. In Proceedings of ASME 2009 Fluids Engineering Division Summer Meeting. ASME (2009)

Gobin, A., Neau, H., Simonin, O, Llinas, J.R., Reiling, V. and Selo, J.L. Fluid dynamic numerical simulation of a gas phase polymerization reactor. Inter. Journal for Numerical Methods in Fluids, Vol 43, pp. 1199-1220 (2003)

Konan, A., Neau, H., Simonin, O., Dupoizat, M. and Le Goaziou, T. Reactive Multiphase Flow Simulation of Uranium Hexaflouride Conversion Reactor, 7th International conference on multiphase flow, ICMF, Tampa, USA (2010)

Neau, H., Laviéville, J. and Simonin, O. NEPTUNE_CFD high parallel computing performances for particle-laden reactive flows, 7th International conference on multiphase flow, ICMF, Tampa, USA (2010)

Simonin, O. Combustion and turbulence in two-phase flows. Lecture Series 1996-02, Von Karman Institute of Fluid Dynamics